FIRST-PRINCIPLES CALCULATIONS OF MÖSSBAUER HYPERFINE PARAMETERS FOR SOLIDS AND LARGE MOLECULES

Diana Guenzburger

Centro Brasileiro de Pesquisas Físicas, rua Xavier Sigaud 150,

22290-180 Rio de Janeiro, RJ, Brasil

D. E. Ellis

Deapartment of Physics and Materials Research Center, Northwestern University,

Evanston, Illinois 60208, U.S.A.

and Z. Zeng

Institute of Solid-State Physics, Academia Sinica, Hefei 230031,

People's Republic of China

ABSTRACT

Electronic structure calculations based on Density Functional theory were performed for solids and large molecules . The solids were represented by clusters of 60-100 atoms embedded in the potential of the external crystal. Magnetic moments and Mössbauer hyperfine parameters were derived.

Key-words: Hyperfine; Solids; Molecules.

I. INTRODUCTION

The theoretical evaluation of the Mössbauer hyperfine parameters Isomer Shift (IS), Quadrupole Splitting (QS) and magnetic Hyperfine Field (H_F) may be performed with first-principles electronic structure calculations based on Density Functional theory (DFT) [1]. The methods employed usually rely on the Local Density approximation (LDA), or Local Spin-Density approximation (LSDA) in the case of magnetic systems [2]. Two types of approaches may be considered. If the solid has translational symmetry, as in a pure crystal, band-structure methods may be employed; these are based on Bloch's theorem, which states that the one-electron wave function ϕ_i at point ($\mathbf{r} + \mathbf{R}$), where $\mathbf{R}$ is a lattice vector, is equal to the function at point $\mathbf{r}$ times a phase factor:

$$\phi_i(\mathbf{r} + \mathbf{R}) = e^{i\mathbf{k}.\mathbf{R}} \phi_i(\mathbf{r}) \qquad (1)$$

The band-structure methods, in which the electronic structure is obtained in $\mathbf{k}$ space, may often be recognized by their initials, such as APW, LMTO, FLAWP, KKR, etc.

On the other hand , if translational symmetry is missing electronic structure calculations may be performed in real space. This applies to molecules containing atoms which are Mössbauer probes such as Fe, Sn, Au, etc, and to solids represented by a cluster of atoms. These solids may be pure crystals or crystals containing inpurities (substitutional or interstitial), vacancies, local geometrical distortions, etc, since no translational symmetry constraints are imposed.

One way of performing DFT calculations in real space is by employing the Discrete Variational method (DVM) [3]. With the DV method it is possible to treat systems of

60-100 atoms , containing transition metals or rare-earths. In the case of clusters representing solids, an embedding scheme is utilized in which the cluster is surrounded by the charge densities of several shells of atoms in the crystal, forming an external potential. In this method the one-electron functions are expanded on a basis of numerical atomic orbitals , and are then expressed on a three-dimensional grid of points.

In section II the main features of the DV method are described briefly, as well as the manner of calculating the hyperfine parameters. In section III are given a few examples , covering a wide diversity of systems, of applications of the method .

II. THEORETICAL METHOD

a. The self-consistent procedure

The self-consistent DVM scheme constitutes of solving iteratively the set of Kohn-Sham equations of DFT [4] for the cluster or the molecule, in a three-dimensional grid of points (in Hartrees):

$$h_{KS}\ \phi_{i\sigma} \equiv (-\nabla^2/2 + V_c + V^{\sigma}_{xc})\phi_{i\sigma} = \varepsilon_{i\sigma}\phi_{i\sigma} \quad (2)$$

where V_c is the Coulomb potential of the nuclei and electrons and V^{σ}_{xc} is the exchange and correlation potential for spin σ [5], functionals of the electron density of spin σ:

$$\rho_\sigma(\mathbf{r}) = \sum_i n_{i\sigma} |\phi_{i\sigma}(\mathbf{r})|^2 \quad . \qquad (3)$$

The self-consistent procedure is the following : an initial density ρ is assumed (usually a superposition of atomic densities) , the Kohn-Sham Hamiltonian h_{KS} in Eq.(2) is constructed and the set of equations is solved. From the eigenvectors ϕ obtained, a new density is derived according to equation (3), a new h_{KS} is formed and the equations are solved again. This procedure is repeated until the ρ obtained is the same as the input ρ, within an established accuracy. The occupation numbers $n_{i\sigma}$ are given by Fermi-Dirac statistics. In spin-polarized calculations $\rho_\uparrow(\mathbf{r})$ has the freedom to be different from $\rho_\downarrow(\mathbf{r})$, thus creating a spin density and magnetic effects.

The molecular or cluster spin-orbitals $\phi_{i\sigma}$ are expanded as linear combinations of numerical atomic orbitals (LCAO or tight-binding approximation). Applying the Discrete Variational scheme leads to the secular equations that are solved self-consistently in the three-dimensional grid:

$$([H] - [E][S])\,[C] = 0 \qquad (4)$$

In Eq. (4), [H] is the Hamiltonian matrix, [S] the overlap matrix and [C] the matrix of the eigenvector coefficients which define $\phi_{i\sigma}$. The numerical grid is pseudo-random (Diophantine), except inside spheres centered around certain atomic nuclei, where a more precise polynomial integration may be necessary, as for the case of calculations of hyperfine interactions. The total number of points per atom varies from 200-300

for small atoms such as C or N, to several thousands for larger atoms such as transition metals and lanthanides.

In the case of clusters representing solids, the embedding is constructed by placing electron densities obtained with atomic calculations at the sites of several shells of atoms in the surrounding crystal. The external densities at each point are added to the cluster density to build the cluster Hamiltonian.

To facilitate the evaluation of the Coulomb term, a model density consisting of a multicenter multipolar expansion is used in the Hamiltonian, and fitted to the "real" density by a least-squares procedure [6].

b. Magnetic and hyperfine parameters

In systems where the number of spin 1/2 electrons exceeds the number of spin -1/2, the exchange-correlation potential V_{xc} in Eq.(2) will be different for each spin. From spin-polarized calculations , the spin density $\rho\uparrow(\mathbf{r}) - \rho\downarrow(\mathbf{r})$ may be obtained at each point **r**. Furthermore , spin magnetic moments at each atomic site may be defined as the total atomic Mulliken population (electron ocupation number) of spin up minus spin down. This definition allows the analysis of the orbitals contributions to the moment; an alternative definition is provided by integrating the spin density inside each atomic volume.

The Isomer Shift (IS) measured by Mössbauer spectroscopy is defined as [7]:

$$IS = 2/3\ e^2\ \pi\ Z\ S'(Z)\ \Delta\langle r^2\rangle\ [\ \rho_A(0) - \rho_S(0)] \quad (5)$$

where $\Delta\langle r^2\rangle$ is the variation of the mean-square radius of the nucleus between the excited and ground states of the Mössbauer transition, S'(Z) is a correction for relativistic effects and the term in brackets is the difference between the electron density at the nucleus in the absorber A and source S. In a non-relativistic approximation, only orbitals containing s states contribute to $\rho(0)$. For ^{57}Fe, a correlation between $\rho(0)$ (3s + 4s) and IS values for free atom and ions gave IS = $-0.228\ \rho(0) + 33.638$ [8].

The quadrupole splitting QS of the excited state of the 14.4 keV transition of ^{57}Fe is given by:

$$QS = 1/2\ e\ V_{zz}\ Q\ (1 + \eta^2/3)^{1/2} \qquad (6)$$

where Q is the quadrupole moment of the nucleus in the excited state (I=3/2) of the Mössbauer transition, V_{zz} the electric field gradient and η the asymmetry parameter , which is zero for axial symmetry. The components of the electric field gradient tensor are calculated from the self-consistent molecular or cluster density by:

$$V_{ij} = -e \int \rho(\mathbf{r})\ (3x_i x_j - \delta_{ij} r^2)/r^5\ dv + \sum_q Z^e_q\ (3x_{qi}\ x_{qj} - \delta_{ij} r^2)/r^5_q + \sum_p K_p\ (3x_{pi}\ x_{pj} - \delta_{ij} r^2)/r^5_p \qquad (7)$$

The first term is the valence electronic contribution, the second term is the contribution of the surrounding nuclei of the cluster or molecular atoms, with effective charge Z^e_q equal to the number of protons minus the number of core electrons, and the

third term is the contribution (only in the case of solids) of the atoms external to the cluster, taken as point charges. After diagonalization , necessary in the absence of axial symmetry, the electric field gradient is defined by the convention:

$$|V_{zz}| > |V_{yy}| \geq |V_{xx}| \quad (8)$$

with $\eta = (V_{xx} - V_{yy})/V_{zz}$. The value of Q employed was 0.16b [9].

The contact or Fermi component H_c of the magnetic hyperfine field H_F , which is usually the dominant component, is given by:

$$H_c = (8/3)\ \pi\ \mu_B\ [\rho\uparrow(0) - \rho\downarrow(0)] \quad (9)$$

where μ_B is the Bohr magneton and the term in brackets is the spin density at the nucleus.

II. MAGNETISM AND HYPERFINE FIELDS IN γ-Fe

Pure bulk γ-Fe (or fcc Fe) only exists at very high temperatures (between 1183 and 1667 K). However, fcc Fe may be stabilized down to very low temperatures either as small coherent precipitates in a Cu or Cu alloy matrix, or as thin epitaxial films on a Cu substrate [10]. There is great interest in fcc Fe due to the existence of several low-lying magnetic states; band structure calculations have shown that at larger

interatomic distances, a ferromagnetic (FM) state is more stable, and at smaller distances an antiferromagnetic (AFM) state prevails [11].

We have performed calculations for 62-atoms clusters representing γ-Fe (see Fig. 1), to investigate the origin of the large difference found experimentally in the magnitude of the hyperfine fields of fcc Fe, which are small at small lattice constants (AFM) and much larger at large lattice constants (FM) [10]. So far, this difference had been ascribed to a large increase in the magnetic moments when changing from AFM to FM. The calculated magnetic moments, plotted in Fig. 2, indeed show a gap between AFM and FM, but not the large differences that would explain the experimental data, obtained by Mössbauer spectroscopy (see Ref. [10]).

On the other hand, the calculated hyperfine fields display a much wider gap (see Fig. 3). Upon separating the valence or conduction electrons contribution (4s) from the core contribution (1s + 2s + 3s), it is verifyed that for AFM γ-Fe the valence contribution is positive and largely cancels the negative core fields, resulting in total fields of small magnitude. On the other hand, for FM the valence contribution is negative and adds to the negative core field, resulting in total fields of much larger magnitude [12].

We conclude that the large difference found experimentally in the magnitude of the hyperfine fields of FM and AFM fcc Fe originates mainly from different signs of the valence electrons contributions, and not from large differences in the Fe magnetic moments in the two states. This result shows clearly that the common practice of considering the hyperfine field as proportional to the magnetic moment may be very misleading.

Calculations were also performed for clusters representing Fe particles in fcc Cu [13] to simulate the precipitates formed experimentally. It was found that the Cu

atoms develop small 3d magnetic moments polarized ferromagnetically with respect to Fe 3d, and 4s,4p moments polarized antiferromagnetically, in agreement with recent magnetic circular dichroism experiments on multilayers [14].

IV. RARE-EARTH BOROCARBIDES: PURE AND Fe-SUBSTITUTED

The rare-earth borocarbides $RENi_2B_2C$ (RE is for rare-earth) have attracted a great deal of attention recently due to the discovery of superconductivity in the case of the heavy RE (Dy, Ho, Er and Tm) [15]. However, it was intriguing that , although the compounds could be synthesized also with the light rare-earths, no superconductivity could be found in the latter.

Spin-polarized calculations were performed for 73-atoms clusters representing the layered borocarbides (RE=Pr, Nd, Sm, Gd, Ho, Tm) (see Fig. 4), to investigate the interplay between magnetism and superconductivity in these compounds [16]. According to experimental findings, the RE layers have FM magnetic order among atoms in the same layer, and AFM among layers. It was found that the conduction electrons spin polarization produced by the RE 4f spin moments is much more effective in the case of the light RE, than in the heavy RE. This result is illustrated in Fig. 5 , where the spin densities of $HoNi_2B_2C$ and $NdNi_2B_2C$ are compared. It may be seen that , although the 4f spin moments are of comparable magnitude in both cases ($3.1\mu_B$ and $3.6\mu_B$ respectively), the spin density of the conduction electrons is much larger and more extended for $NdNi_2B_2C$. The reason for this is that the radius of the 4f orbital of the RE contracts rapidly along the series, and thus for the heavier RE it does not polarize the valence electrons effectively. The spin density of the valence electrons create an exchange field that tends to destroy the Cooper pairs, which are

singlets; since this spin density was calculated to be considerably larger in the light rare-earth compunds, this explains why no superconductivity could be found in the latter.

Clusters similar to the above were considered to represent dilute Fe-substituted $RENi_2B_2C$ (RE=Y, Gd, Tb, Dy, Ho, Er) , with Fe substituting one Ni atom and placed at the center of the cluster. In a theoretical-experimental colaboration [17], calculated quadrupole splittings at the Fe impurity were compared to the values measured by Mössbauer spectroscopy. In Fig. 6 are displayed the theoretical and experimental values, correlated to the ratio of the lattice parameters **c/a.** It is seen that calculated values compare well with experiment. The sign of the electric field gradient, which was not obtained experimentally except for Ho, was found to be negative in all cases. Furthermore, the almost linear correlation with **c/a** was discovered to be due to a volume effect, and not to a chemical effect brought in by RE substitution. In fact, as demonstrated theoretically for $Gd(Ni_{0.99}Fe_{0.01})_2B_2C$ [17], a decrease in the lattice parameter **a** (along the Ni plane) diminishes dramatically the magnitude of QS.

V. NANOSCALE Fe-O MOLECULAR CLUSTERS

Systems of nanoscale or mesoscopic dimensions containing a finite number of transition-metal atoms display a number of interesting or unusual magnetic properties, since they may be considered to be on the borderline of isolated and collective magnetic behavior [18]. Among the properties found are superparamagnetism and macroscopic quantum tunnelling; furthermore, they have been the subject of investigations focused on technological applications, such as magnetic refrigeration and more efficient magnetic recording.

One way of obtaining such nanoscale systems with a controlled number of transition metal atoms is the synthesis of nanoscale molecules consisting of a core of transition elements bound to O or S, surrounded by a “crown” of organic ligands. These ligands prevent any further growth of the internal core, and also assure that the magnetic interactions in the molecular crystal will be confined to the interior of each molecule, such that any collective effects found will be solely due to the nanoparticle. Furthermore, such molecules may be considered to be models for ferritin, a protein found in mammals which is responsible for Fe storage.

A number of such nanomolecules containing Fe have been investigated with Mössbauer spectroscopy, which gives valuable information on chemical bonding and magnetic properties [19]. Electronic structure calculations were performed for two large Fe molecules [20]: $[Fe(OMe)_2(O_2CCH_2Cl)]_{10}$, denominated “ferric wheel” due to the circular disposition of the 10 Fe atoms [21], and $[Fe_{11}O_6(OH)_6\ (O_2CPh)_{15}]$ [22]. In the case of the “ferric wheel” (Fig. 7), all atoms were included except the terminal H and Cl; as for $[Fe_{11}O_6(OH)_6\ (O_2CPh)_{15}]$ (Fig. 8) , the C-O bonds of the benzoate ligands were truncated, and the organic ligands substituted by H , a procedure known as “Hydrogen saturation”.

In Table I are given the results of the magnetic moments and Mössbauer parameters for both molecules. For the “ferric wheel”, the magnetic moment is somewhat smaller than what would be expected for a Fe +3 ion; the agreement between the calculated and experimental values of IS and QS is good. For $[Fe_{11}O_6(OH)_6\ (O_2CPh)_{15}]$, three different types of Fe are present. Experimental evidence [22] points to an antiferromagnetic configuration; for comparison, both FM and a model AFM states were considered in the calculations. It is seen that for the AFM configuration the agreement between calculated and experimental values of the hyperfine parameters is

good, although the theoretical IS values are somewhat higher than experiment. Calculations of the magnetic hyperfine field for this molecule are in progress.

Acknowledgments

Calculations were performed at the Cray Y-MP of the Supercomputing Center of the Universidade Federal do Rio Grande do Sul, and at the Cray J90 of COPPE/Universidade Federal do Rio de Janeiro.

TABLE I

Magnetic moments, isomer shifts and quadrupole splittings of nanoscale Fe molecules

$[Fe(OMe)_2(O_2CCH_2Cl)]_{10}$ ("ferric wheel")

	calculated	experimental [a]
Magnetic Moment (μ_B)	4.3	--
Isomer Shifts (mm/s)	0.48	0.52
Quadrupole Splittings (mm/s)	+0.73	0.62

$[Fe_{11}O_6(OH)_6(O_2CPh)_{15}]$

		AFM calculated	experimental[b]
Magnetic Moment (μ_B)	A	4.14	--
	B	3.67	--
	C	3.66	--
Isomer Shift (mm/s)	A	0.74	0.53
	B	0.78	0.46
	C	0.82	0.51
Quadrupole Splitting (mm/s)	A	–0.52	0.49
	B	–0.83	0.87
	C	–1.78	1.10

a) From reference [21]. The sign of QS was not determined.
b) From reference [22]. The sign of QS was not determined.

FIGURE CAPTIONS

Figure 1:

62-atom cluster representing fcc Fe. The AFM configuration considered (layered) is represented by different spheres shades.

Figure 2:

Magnetic moments μ plotted against the Wigner-Seitz radius r_s for fcc Fe. From ref.[12]

Figure 3:

Hyperfine field and components plotted against the Wigner-Seitz radius r_s Conduction electrons contribution . . . . . ; core electrons contribution - - - - - - - - -; total _____. From ref. [12].

Figure 4:

73-atoms cluster representing $RENi_2B_2C$.

Figure 5:

Spin density contours on a diagonal plane along the **c** direction for $NdNi_2B_2C$ and $HoNi_2B_2C$ (see ref. [16]). Positive spin density _____; negative - - - - - - .

Figure 6:

Experimental and calculated absolute values of QS of $RE(Ni_{0.99}Fe_{0.01})_2B_2C$ against **c/a.** From ref. [17].

Figure 7:

Representation of the molecule $[Fe(OMe)_2(O_2CCH_2Cl)]_{10}$ (Cl and H excluded) .

Figure 8:

Representation of the molecule $[Fe_{11}O_6(OH)_6\ (O_2CPh)_{15}]$ (Fe-O core only).

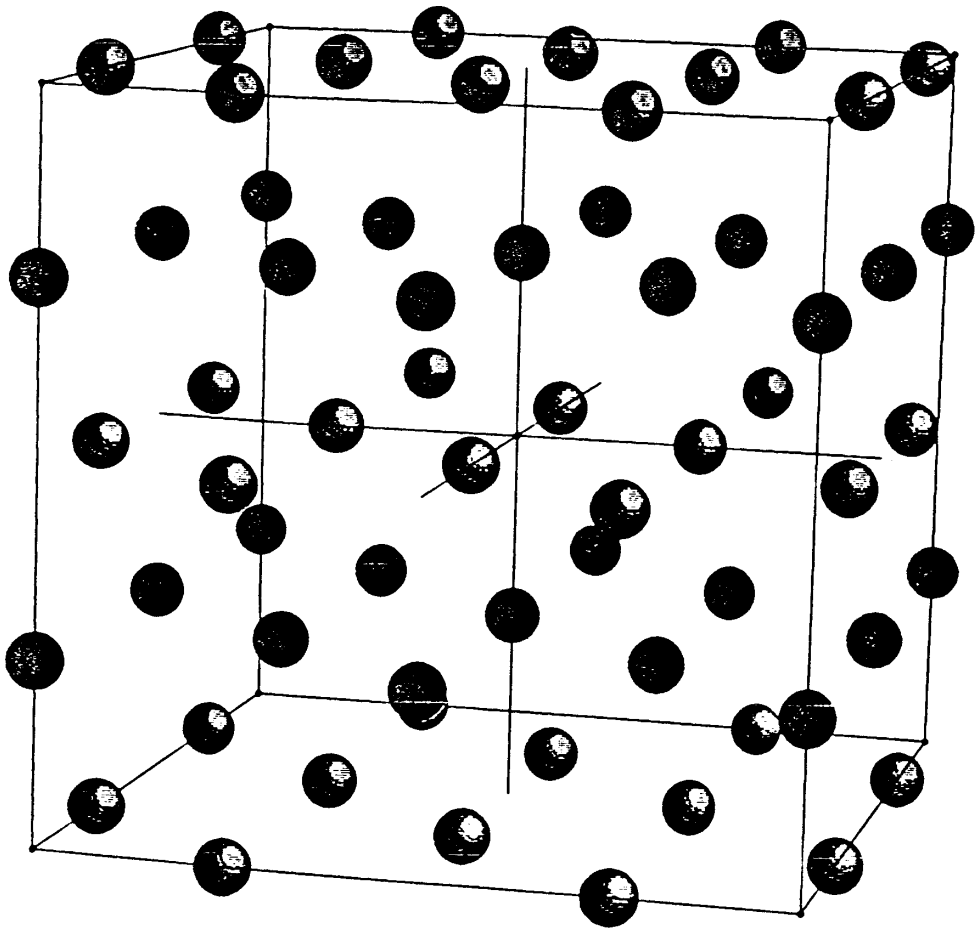

Figure 1

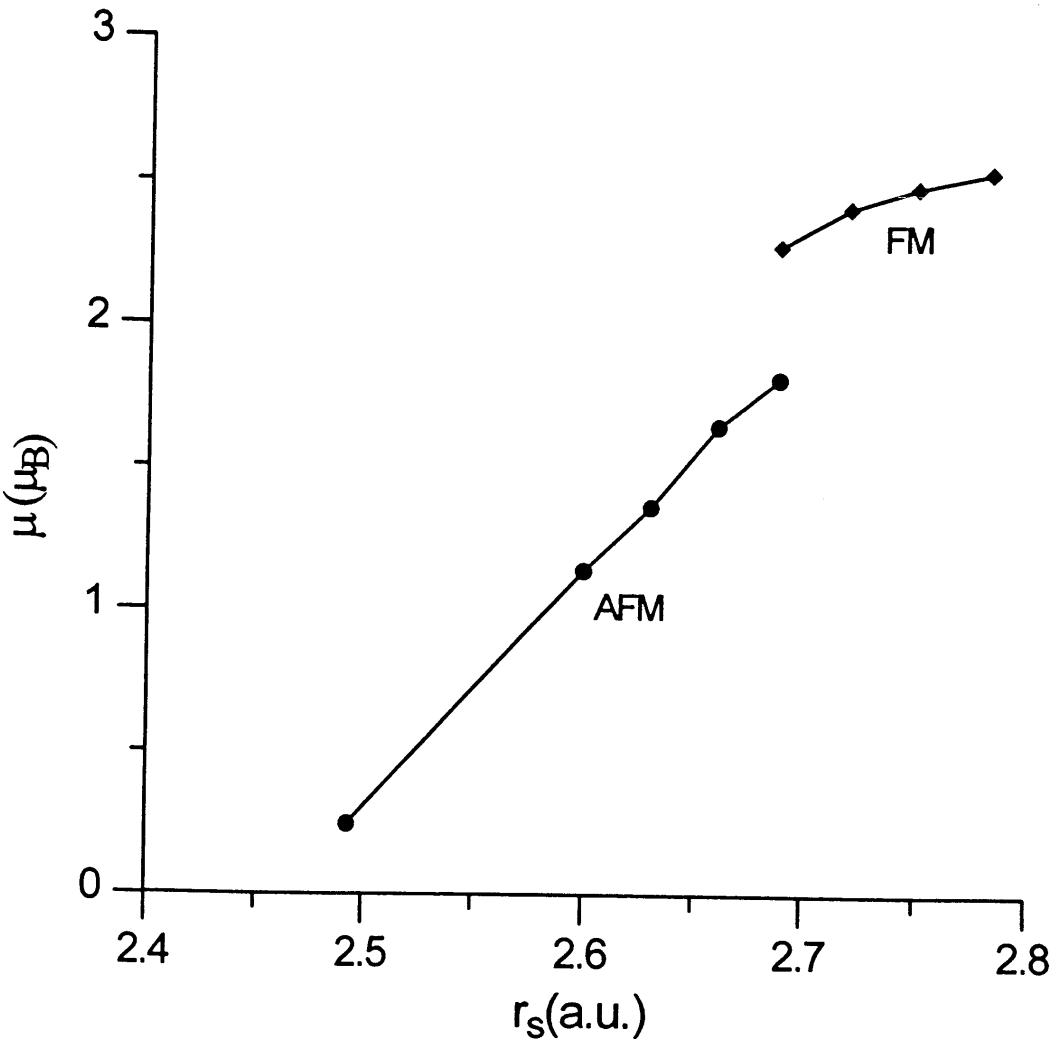

Figure 2

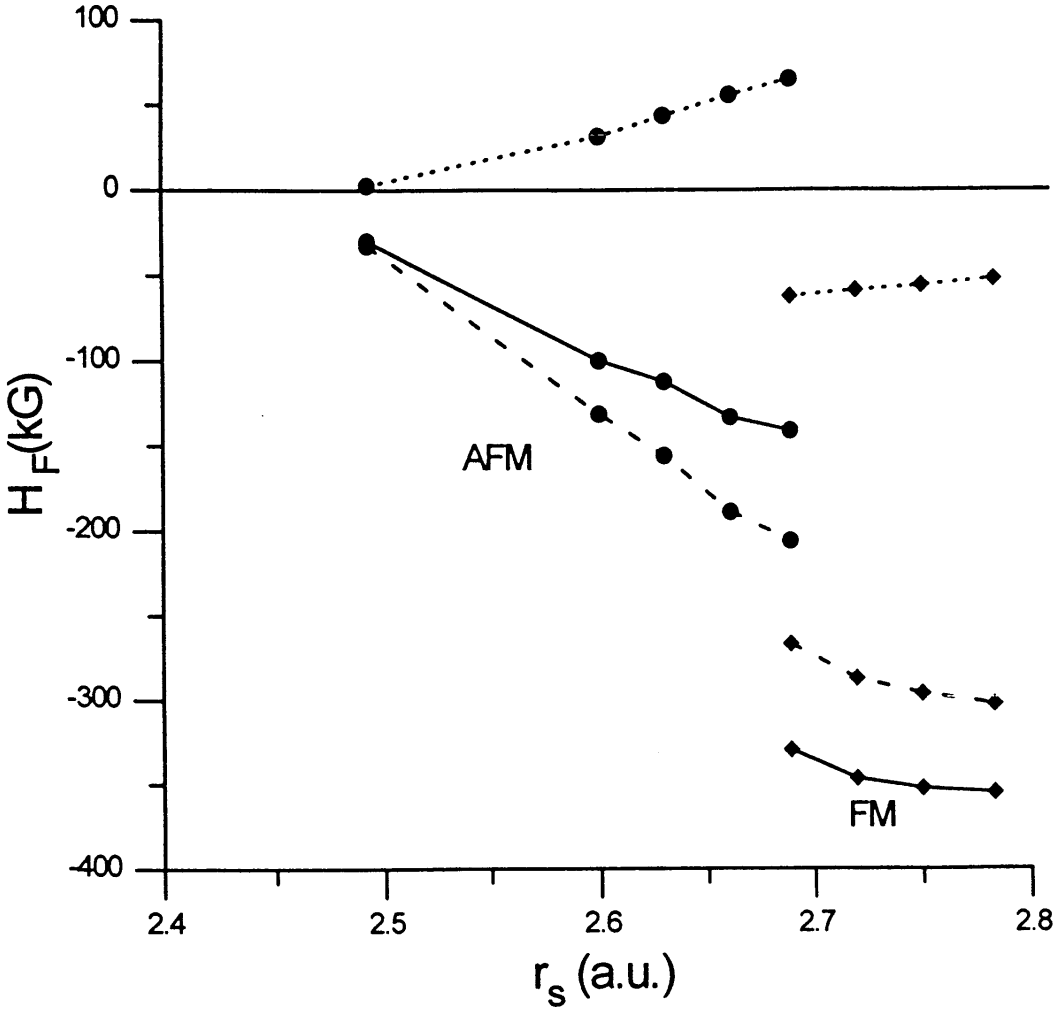

Figure 3

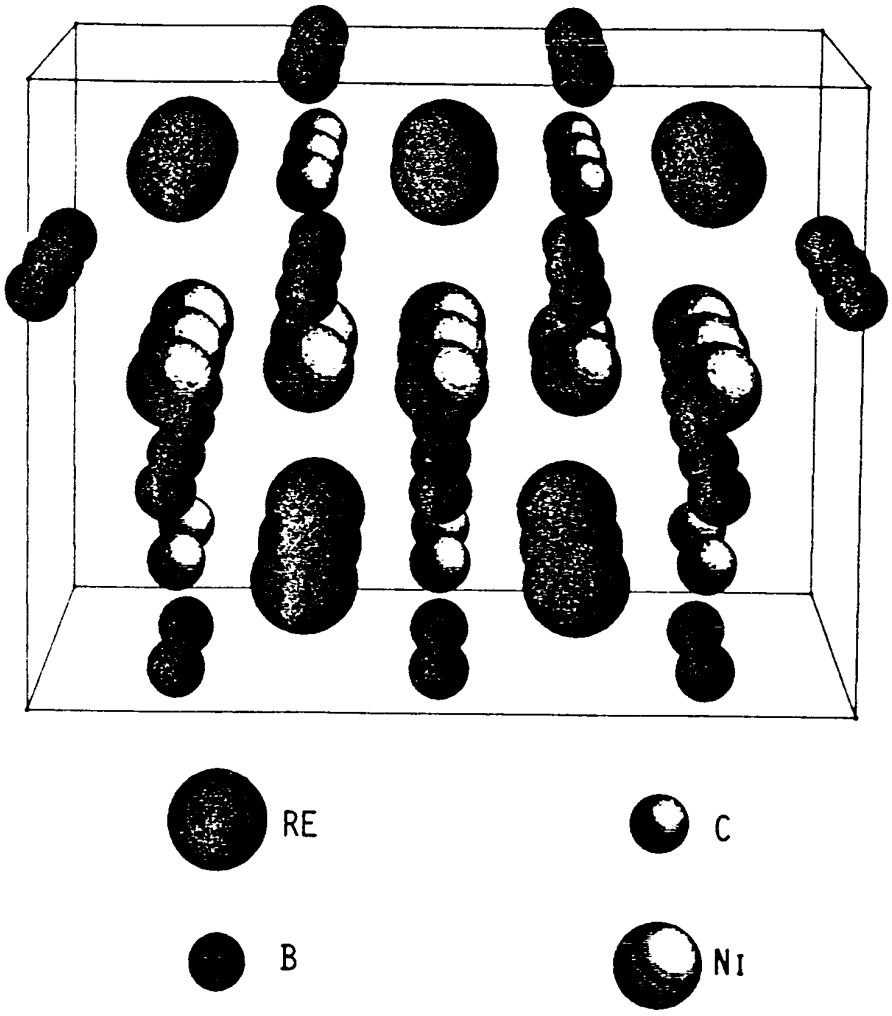

Figure 4

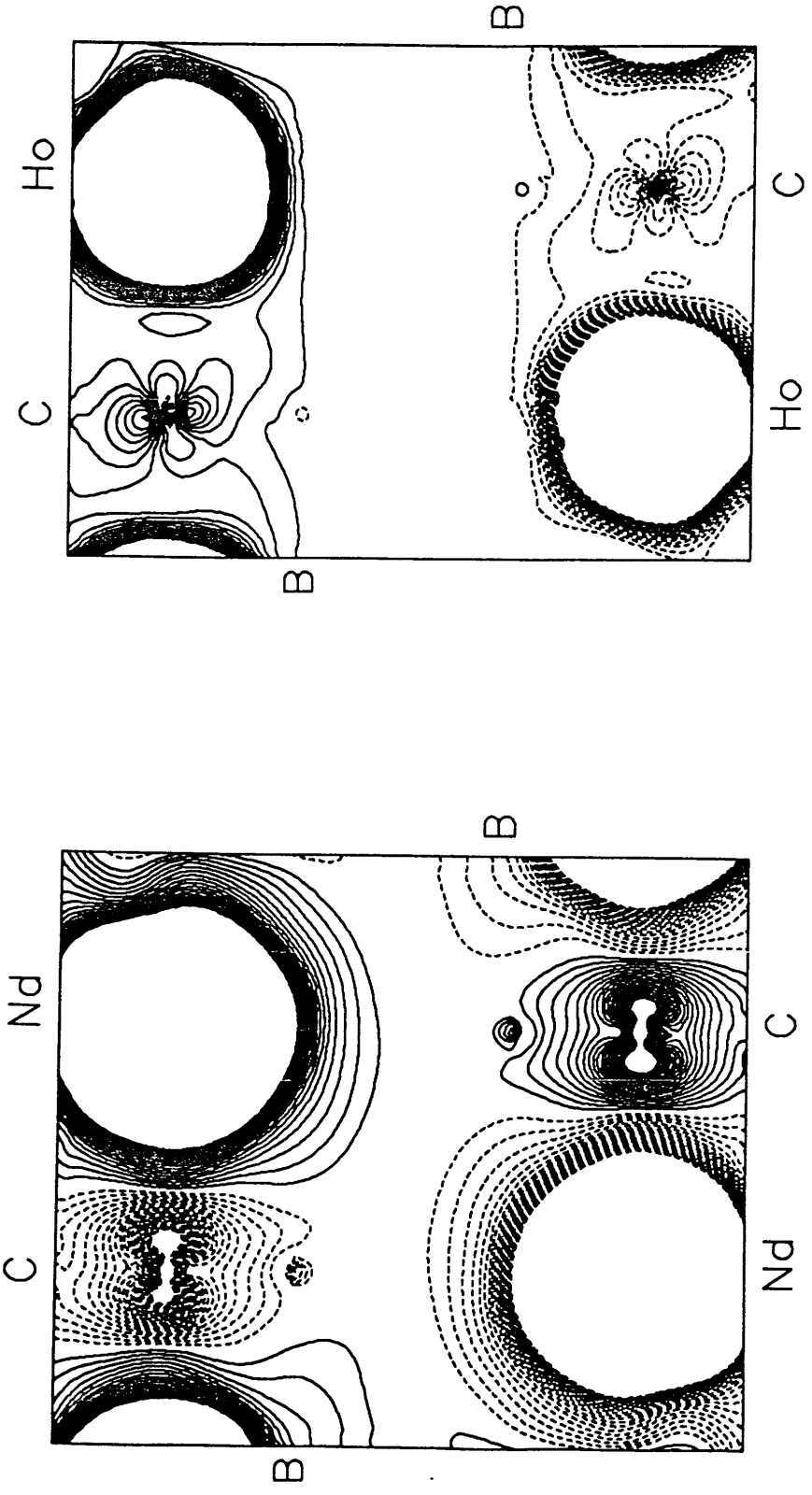

Figure 5

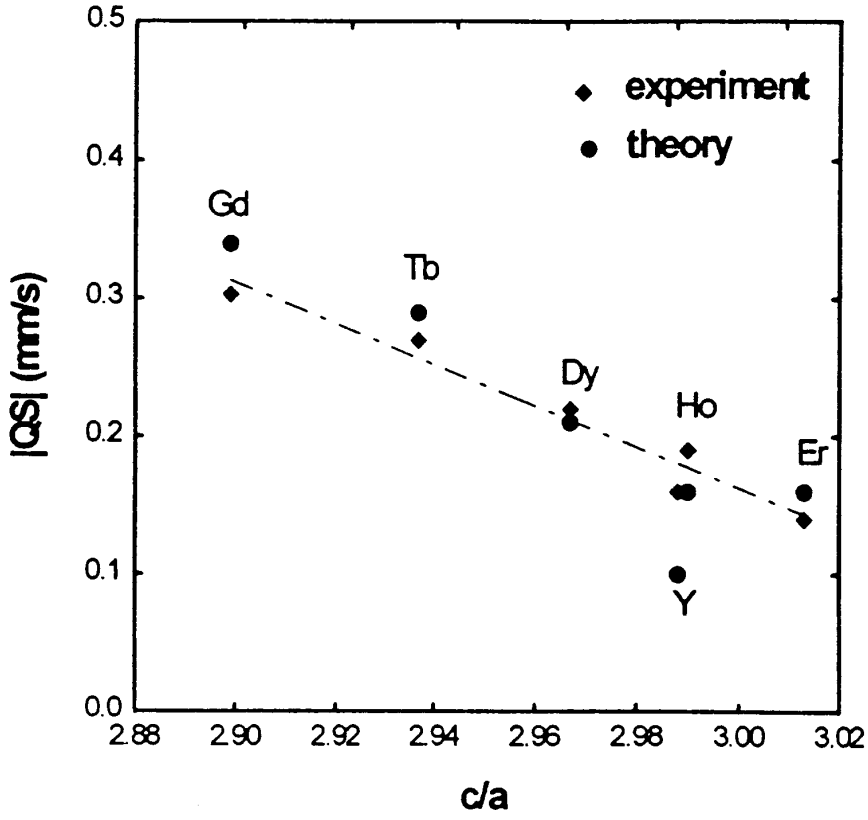
experiment
theory
Gd
Tb
Dy
Ho
Er
Y
|QS| (mm/s)
c/a
0.0
0.1
0.2
0.3
0.4
0.5
2.88
2.90
2.92
2.94
2.96
2.98
3.00
3.02

Figure 6

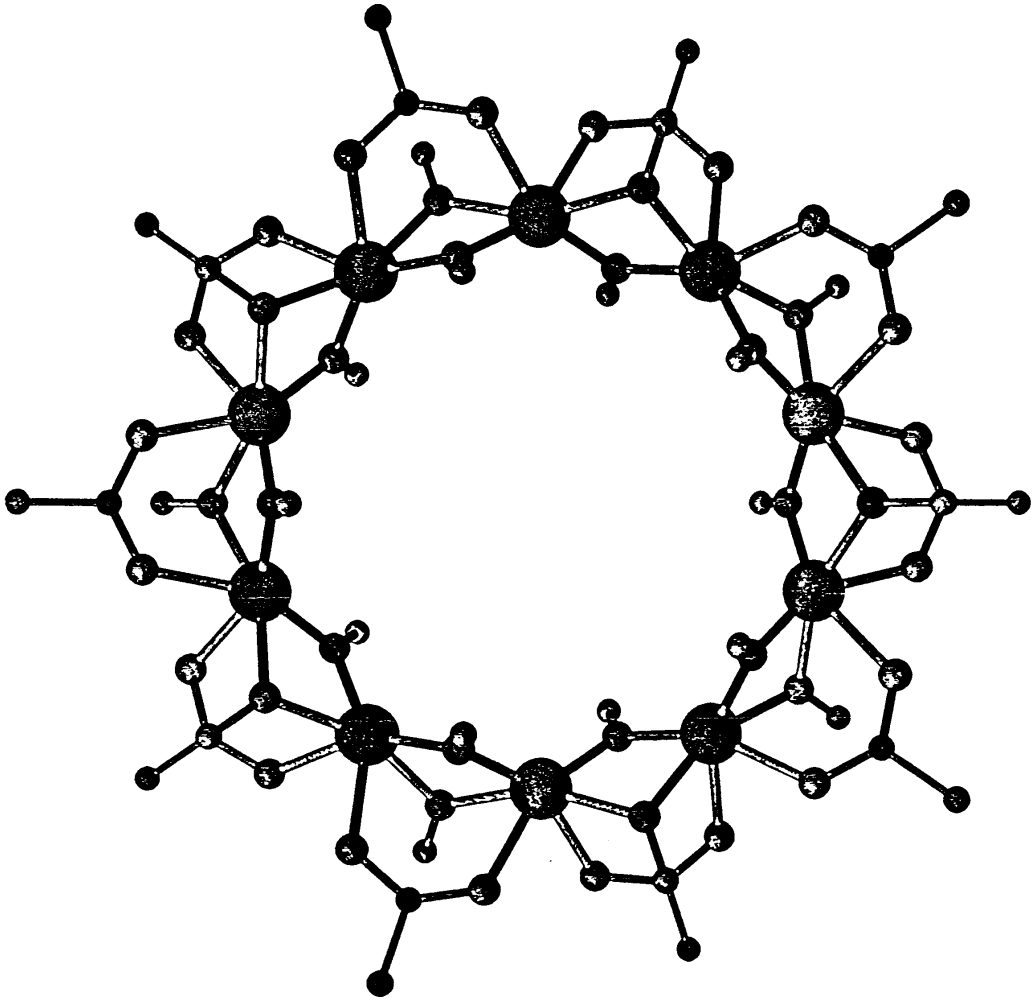

Figure 7

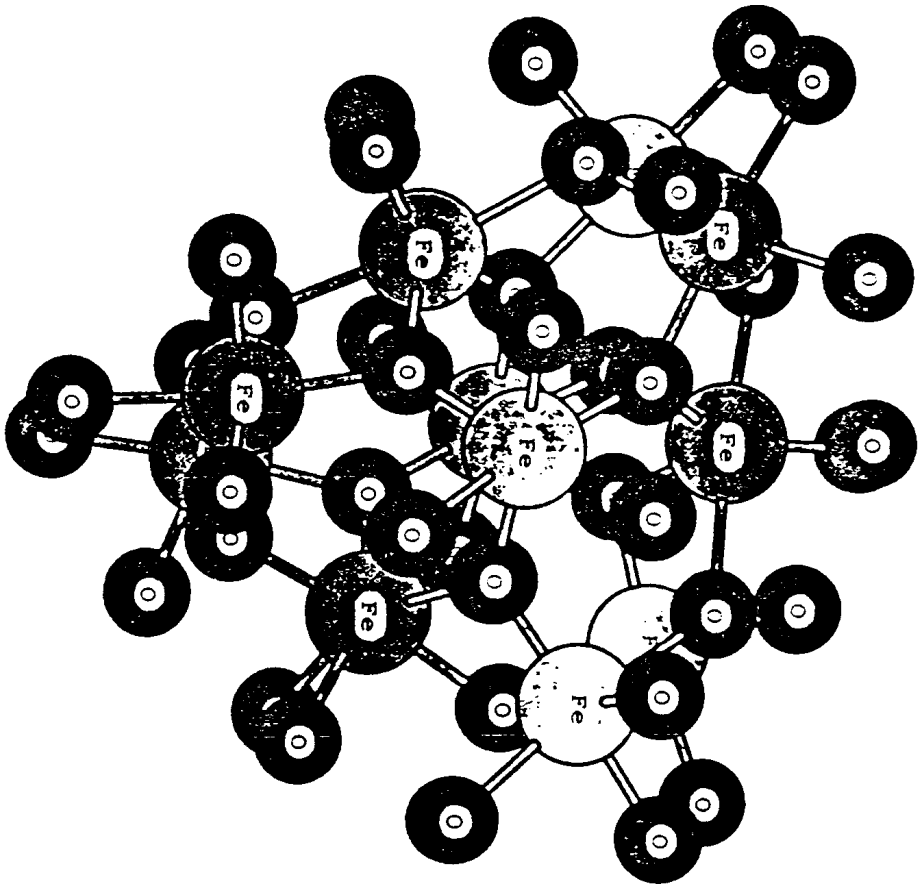

Figure 8

REFERENCES

1) See, for example: R.G. Parr and W. Yang, *Density Functional Theory of Atoms and Molecules* (Oxford University Press, New York, 1989).
2) R. O. Jones and O. Gunnarsson, Rev. Mod. Phys. 61 (1989) 689.
3) D. E. Ellis, Int. J. Quant. Chem. S2 (1968) 35; D. E. Ellis and G. S. Painter, Phys. Rev. B 2 (1970) 2887.
4) W. Kohn and L. J. Sham, Phys. Rev. 140 (1965) A1133.
5) U. von Barth and L. Hedin, J. Phys. C 5 (1972) 1629.
6) B. Delley and D. E. Ellis, J. Chem. Phys. 76 (1982) 1949.
7) N. N. Greenwood and R. C. Gibb, *Mössbauer Spectroscopy* (Chapman and Hall, London, 1971).
8) J. Terra and D. Guenzburger, J. Phys. Chem. 99 (1995) 4935.
9) P. Dufek, P. Blaha and K. Schwarz, Phys. rev. Letters 75 (1995) 3545.
10) W. Keune, T. Ezawa, W. A. A. Macedo, U. Glos and K. P. Schletz, Physica B 161 (1989) 269.
11) C. S. Wang, B. M. Klein and H. Krakauer, Phys. Rev. Letters 54 (1985) 1852.
12) D. Guenzburger and D. E. Ellis, Phys. Rev. B 51 (1995) 12519.
13) D. Guenzburger and D. E. Ellis, Phys. Rev. B 52 (1995) 13390.
14) S. Pizzini, A. Fontaine, C. Georgetti, E. Dartyge, J.-F. Bobo, M. Piecuch and F. Baudelet, Phys. Rev. Letters 74 (1995) 1470, and references therein.
15) B. K. Cho, P. C. Caulfield and D. C. Johnston, Phys. Rev B 52 (1995) R3844, and references therein.
16) Z. Zeng, D. Guenzburger, D. E. Ellis and E. M. B. Saitovitch, Physica C 271 (1996) 23.
17) Z. Zeng, D. R. Sánchez, D. Guenzburger, D. E. Ellis, E. M. B. Saitovitch and H. Micklitz, Phys. Rev. B 55 (1997) 3087.
18) D. D. Awschalom and D. P. DiVincenzo, Phys. Today 48 (1995)43.
19) G. C. Papaefthymiou, Phys. Rev. B46 (1992) 10366.
20) Z. Zeng, Y. Duan and D. Guenzburger, Phys. Rev. B 55 (1997) 12522.
21) K. L. Taft, C. D. Delfs, G. C. Papaefthymiou, S. Foner, D. Gatteschi and S. Lippard, J. Am. Chem. Soc. 116 (1994) 823.
22) S. M. Gorun, G. c. Papaefthymiou, R. B. Frankel and S. J. Lippard, J. Am. Chem. Soc. 109 (1987) 3337.